S. C. Du
Graduate Assistant.

B. J. Huang
Professor.

R. H. Yen
Professor.

Department of Mechanical Engineering,
National Taiwan University,
Taipei, Taiwan 10764,
Republic of China

Hydrodynamic Instability of Solar Thermosyphon Water Heaters

The flow instability of a solar thermosyphon water heater is studied analytically. A system dynamics model is derived by means of a one-dimensional approach and a linear perturbation method. The characteristic equation is obtained and the Nyquist criterion is used to examine the flow stability. The parameter M *is a dimensionless parameter of system stability. The stability maps are plotted in terms of 14 parameters. The occurrence of hydrodynamic instability is determined by comparing the stability curves and the designed values of* M. *Flow instability is shown not to occur in most of solar water heaters commercially available, because the loop friction is relatively high in the design and because solar irradiation in field operation is still not high enough to cause flow instability.*

1 Introduction

The phenomenon of reverse flow has been observed in solar thermosyphon water heaters. Reverse flow can reduce the overall efficiency and thus should be avoided. Two kinds of reverse-flow mechanisms are noted: namely, thermosyphon saturation and hydrodynamic instability. The reverse flow due to thermosyphon saturation results mainly from reverse of the thermosyphon head during periods of low irradiation or at a relatively high rate of cooling of the collector side. Reverse flow of this kind can be suppressed by increasing the vertical distance between the tank bottom and the collector top (Vaxman and Sokolov, 1986; Morrison, 1986).

Reverse flow caused by hydrodynamic instability for thermosyphon loops of simple geometry has been studied (for example, Greif, 1988; Welander, 1967; Keller, 1966; Creveling et al., 1975; Bau and Torrance, 1981; Huang and Zelaya, 1987). Flow instability may occur and finally results in reverse flow in the thermosyphon loops under certain operating conditions. It had thus been suspected that hydrodynamic instability may also exist and causes flow reverse in solar systems as the solar thermosyphon water heater is a kind of thermosyphon loop.

To study analytically the stability of the solar thermosyphon water heaters, Zvirin et al. (1978) used linear system theory and assumed linear distribution functions for the perturbed (transient) components of the temperatures in the collector and the tank (or the heat exchanger situated in the tank) which leads to a simple characteristic equation of the system. This assumption is not exactly true since it implies that the response of the collector temperature to the variation of solar radiation is instantaneous. Zvirin and Greif (1979) used the same assumption to study a simple thermosyphon loop that was investigated by Welander (1967), but they failed to verify the hydrodynamic instability predicted by Welander and attributed this error to the assumption of linear distribution function for the perturbed temperatures.

The present study was to investigate the existence of hydrodynamic instability in the thermosyphon water heater. Instead of using the approximation of Zvirin et al., a system dynamics model is derived analytically by using a one-dimensional approach and linear perturbation method. A system transfer function, which treats the solar irradiation as the system input and the flow rate as the system output, is derived to represent the system dynamics behavior of solar thermosyphon water heaters. The characteristic equation is then obtained and the Nyquist criterion is used to examine the flow instability. The analysis is then tested by the numerical solutions in the time domain. Dimensionless parameters related to flow instability are derived and stability maps are constructed and used to determine the occurrence of instability.

2 Governing Equations

The solar thermosyphon water heater studied is a *closed loop*, similar to that of Mertol et al. (1981) (Fig. 1). A heat exchanger is designed in the tank to extract indirectly the solar energy absorbed in the collector so that the freezing problem can be avoided by using a working fluid of low frozen point inside the natural circulation loop. In the derivation of the governing equations we have made the following assumptions:

(1) A two-node dynamic model is used for the collector. That is, the collector is assumed to be composed of a solid phase (absorber plate) and a fluid phase.

(2) The heat capacity effects of the connecting pipe and exchangers walls are ignored.

(3) The convective heat-transfer coefficients and the physical properties of the circulating fluid (water), except the density in the derivation of buoyancy term in the momentum equation, are all constant.

(4) The axial conduction of the plate and of the fluid along the flow direction is negligible.

From assumption (3), the conservation of mass yields $\dot{m} = \dot{m}(t)$. The energy equations derived for the loop are

$$\rho_p A_p C_{pp} \frac{\partial T_p}{\partial t} = Q - U_a(T_p - T_a) - U_w(T_p - T_w), \quad \text{for collector plate} \quad (1)$$

Contributed by the Solar Energy Division of THE AMERICAN SOCIETY OF MECHANICAL ENGINEERS for publication in the ASME JOURNAL OF SOLAR ENERGY ENGINEERING. Manuscript received by the ASME Solar Energy Division, Apr. 29, 1992; final revision Aug. 3, 1993. Associate Technical Editor: Z. Lavan.

$$\rho_w A C_{pw}\frac{\partial T_w}{\partial t}+\dot{m}C_{pw}\frac{\partial T_w}{\partial y}$$

$$=\begin{cases} U_w(T_p-T_w), & \text{where } A=A_w \text{ for fluid in the collector} \\ -U_p(T_w-T_a), & \text{where } A=A_u \text{ for fluid in the riser} \\ -U_e(T_w-T_t), & \text{where } A=A_e \text{ for fluid in the exchanger} \\ -U_p(T_w-T_a), & \text{where } A=A_d \text{ for fluid in the downcome} \end{cases} \tag{2}$$

The momentum equation of the loop is

$$F_{tm}\frac{d\dot{m}}{dt}=\oint T_w\mathbf{e}_y\cdot\mathbf{e}_z dy-F_{fm}\cdot\dot{m}^d, \tag{3}$$

where

$$F_{tm}=\frac{1}{\rho_w g\beta}\left(\frac{L_c}{A_w}+\frac{L_u}{A_u}+\frac{L_e}{A_e}+\frac{L_d}{A_d}\right), \quad F_{fm}=\frac{c}{\beta}. \tag{4}$$

The derivation of Eq. (3) uses relation for the frictional head that is expressed by a semi-empirical formula $H_f=c\cdot\dot{m}^d$, where c and d are coefficients determined by a loop friction test suggested by Huang and Hsieh (1985).

The above equations can be separated into the steady-state and perturbed parts according to the linear perturbation method and expressed in the normalized form:

(a) for the steady-state:

$$0=\bar{q}-u_a\bar{\theta}_p-(\bar{\theta}_p-\bar{\theta}_w), \quad \text{collector plate} \tag{5}$$

$$\bar{f}\frac{d\bar{\theta}_w}{dx}=\begin{cases} \bar{\theta}_p-\bar{\theta}_w, & \text{collector} \\ -u_p\bar{\theta}_w, & \text{riser} \\ -u_e(\bar{\theta}_w-\bar{\theta}_t), & \text{exchanger} \\ -u_p\bar{\theta}_w, & \text{downcomer} \end{cases} \tag{6}$$

$$\oint\bar{\theta}_w\mathbf{e}_x\cdot\mathbf{e}_z dx=w_{fm}\bar{f}^d, \quad \text{momentum} \tag{7}$$

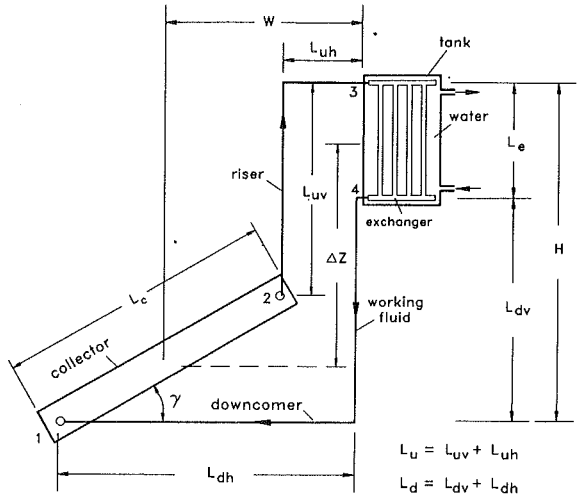

Fig. 1 Closed-loop thermosyphon solar hot water system

(b) for the perturbed state:

$$r_p\frac{\partial\theta_p'}{\partial\tau}=q'-u_a\theta_p'-(\theta_p'-\theta_w'), \quad \text{collector plate} \tag{8}$$

$$r\frac{\partial\theta_w'}{\partial\tau}+f'\frac{\partial\bar{\theta}_w}{\partial x}+\bar{f}\frac{\partial\theta_w'}{\partial x}$$

$$=\begin{cases} \theta_p'-\theta_w', & \text{where } r=r_w, \text{ collector} \\ -u_p\theta_w', & \text{where } r=r_u, \text{ riser} \\ -u_e\theta_w', & \text{where } r=r_e, \text{ exchanger} \\ -u_p\theta_w', & \text{where } r=r_d, \text{ downcomer} \end{cases} \tag{9}$$

$$\frac{w_{tm}}{w_{fm}}\frac{df'}{d\tau}=\frac{1}{w_{fm}}\oint\theta_w'\mathbf{e}_x\cdot\mathbf{e}_z dx-d\cdot\bar{f}^{d-1}f', \quad \text{momentum.} \tag{10}$$

Nomenclature

A_c = area of collector, m^2
A = cross-section area of pipe, m^2
C_p = specific heat, kJ/kg °C
c = coefficients of friction loss head
d = coefficients of friction loss head
$\mathbf{e}$ = unit vector
F = coefficient in momentum equation
F_R = plate heat removal factor
F' = plate efficiency factor
f = flow rate, dimensionless
g = acceleration of gravity, m/s^2
H = height of thermosyphon system, m
H_f = loop friction head, m
h = thermosyphon head of each component, dimensionless
I = solar irradiation on collector slope, W/m^2
L = length, m
M = stability parameter, dimensionless
L_s = length of whole loop, m
$\dot{m}$ = mass flow rate, kg/s
N_u = Nusselt number
n_e = number of tubes in exchanger
Q = solar energy input per unit length of collector, W/m; $Q = IA_c(\tau\alpha)_e/L_c$
q = heat input per unit length, dimensionless
r = time constant, dimensionless
T = temperature, °C
t = time, s
U = heat-transfer coefficient per unit length, W/m °C
U_L = heat loss coefficient of collector, W/m^2 °C
u = heat-transfer coefficient per unit length, dimensionless
W = width of the thermosyphon system, m
w = coefficient in momentum equation, dimensionless
x = coordinate along the loop, dimensionless
y = coordinate along the loop, m
ρ = density, kg/m^3
γ = collector tilt angle, deg
β = thermal expansion coefficient of water, $°C^{-1}$
ϕ = dimensionless variable
ψ = time constant, s
τ = time, dimensionless
θ = temperature, dimensionless
$(\tau\alpha)$ = transmittance-absorptance product of collector
ΔZ = relative height between exchanger and collector, m
Δz = relative height between exchanger and collector, dimensionless
$\bar{}$ = steady-state value
$'$ = perturbed value

Subscripts

a = ambient
c = collector
cr = critical state
d = downcomer
dv = vertical part of downcomer
e = heat exchanger, effective
fm = friction head in momentum equation
n = solar normal incidence
p = collector plate, pipe of riser, and downcomer
ref = reference state
t = tank
tm = inertia in momentum equation
u = riser
uv = vertical part of riser
w = water
x = loop tangent direction, for dimensionless coordinate
y = loop tangent direction
z = gravity direction

Equations (5) to (10) are the governing equations. The dimensionless variables are defined in Appendix A. The water in the tank (different from the working fluid inside the exchanger) is assumed to be well mixed with a uniform temperature since both the mass of water contained in the tank and the thermal mixing effect is large.

3 Analytical Solution

3.1 Steady-State Solutions. An implicit solution for the flow-rate of the working fluid $\bar{f}$ is obtained by solving the steady-state equations

$$w_{fm}\bar{f}^d = \bar{h}_c(\bar{f}) + \bar{h}_u(\bar{f}) - \bar{h}_e(\bar{f}) - \bar{h}_d(\bar{f}). \tag{11}$$

The variables $\bar{h}$'s represent the thermosyphon heads in the various components which are presented in Appendix B. Equation (11) is solved for $\bar{f}$ numerically by iteration.

By assuming a linear steady-state temperature distribution for the working fluid in the collector and exchanger (Ong, 1974; Zvirin et al., 1977), we obtain an explicit solution for the flow rate:

$$\bar{f} = M^{1/(d+1)}; \quad \text{where} \quad M = \frac{\phi \cdot \Delta z}{w_{fm}};$$

$$\phi = \frac{l_c(\bar{q} - u_a\bar{\theta}_t)}{(1+u_a) + l_c u_a / l_e u_e}; \quad \Delta z = \frac{l_{uv} + l_{dv}}{2}. \tag{12}$$

Here M is a parameter that determines the flow rate of the working fluid in the steady-state; ϕ is related to heat transfer in both the collector and the heat exchanger; Δz represents the height of the collector relative to the exchanger or tank; w_{fm} represents the system friction in the steady-state.

3.2 System Dynamics Model. Taking Laplace transform of the perturbed Eqs. (5) to (10) with zero initial conditions and solving analytically, we obtain the transfer function of the system

$$\frac{f'(s)}{q'(s)} = G(s) = \frac{G_n(s)}{G_d(s)},$$

where $G_d(s)$ and $G_n(s)$ are the denominator and numerator of $G(s)$ defined as

$$G_d(s) \equiv c_1 \left\{ w_{fm} \left(\frac{w_{tm}}{w_{fm}} s + d\bar{f}^{d-1} \right) s c_1 c_4 c_5 c_6 c_7 (1 - p_1 p_2 p_3 p_4) - (h_c' + h_u' - h_e' - h_d') \right\} \tag{13}$$

$$G_n(s) \equiv c_3 \cdot (h_{qc}' + h_{qu}' - h_{qe}' - h_{qd}'). \tag{14}$$

All variables in the above equations are presented in Appendix C. The flow rate $f'(s)$ is the system output which is induced by solar radiation q' (the input).

System stability is then determined according to the unstable roots of $G_d(s)$. That is, the characteristic equation of the system is

$$G_d(s) = 0. \tag{15}$$

3.3 Stability Analysis. According to the Nuquist criterion, if $G_d(s)$ has roots in a finite region bounded by a closed contour C_s along a clockwise direction in the s-domain, the mapping contour of $G_d(s)$ from C_s will encircle the origin in a clockwise direction. As $G_d(s)$ is a transcendental function, the number of roots are infinite. However, the flow response in solar thermosyphon water heaters is generally slow; that is, a solar thermosyphon system behaves as a low-pass filter. The responses at high frequencies are therefore beyond the range of practical applications. It is thus unnecessary to examine the unstable roots in the high-frequency regions. A finite region bounded by a C_s contour that covers a frequency up to 0.5 rad/s is used to examine the existence of unstable roots. It will be shown later that the frequencies of all unstable roots are typically smaller than 0.1 rad/s.

3.4 Wave-Equation Form of the Governing Equations. The term $\partial\bar{\theta}_w/\partial x$ in the perturbed Eq. (9) is obtained from the steady-state solutions. Equation (9) is further written as in a wave equation form

$$\frac{\partial\theta_w'}{\partial\tau} + \begin{pmatrix} \alpha_w \\ \alpha_u \\ \alpha_e \\ \alpha_d \end{pmatrix} \frac{\partial\theta_w'}{\partial x} + \begin{pmatrix} \xi_w \\ \xi_u \\ \xi_e \\ \xi_d \end{pmatrix} \theta_w' + \begin{pmatrix} \lambda_w \exp\left[\dfrac{-u_a x}{\bar{f}(1+u_a)}\right] \\ \lambda_u \exp(-u_p x/\bar{f}) \\ \lambda_e \exp(-u_e x/\bar{f}) \\ \lambda_d \exp(-u_p x/\bar{f}) \end{pmatrix} f' = \begin{pmatrix} \eta_w, & \text{collector} \\ 0, & \text{riser} \\ 0, & \text{exchanger} \\ 0, & \text{downcomer} \end{pmatrix} \tag{16}$$

where

$$\alpha_w = \bar{f}/r_w, \quad \alpha_u = \bar{f}/r_u, \quad \alpha_e = \bar{f}/r_e, \quad \alpha_d = \bar{f}/r_e$$
$$\xi_w = 1/r_w, \quad \xi_u = u_p/r_u, \quad \xi_e = u_e/r_e, \quad \xi_d = u_p/r_d$$
$$\lambda_w = -k_1/r_w, \quad \lambda_u = -k_2/r_u,$$
$$\lambda_e = -k_3/r_e, \quad \lambda_d = -k_4/r_d \tag{17}$$

$$\eta_w = \frac{1}{r_p r_w} \exp[-(1+u_a)\tau/r_p] \times \left\{ \int_0^\tau \exp[(1+u_a)v/r_p][q'(v) + \theta_w'(x,v)]dv \right\}. \tag{18}$$

Relative to the standard one-dimensional wave equation with wave speed α,

$$\frac{\partial\theta_w'}{\partial\tau} + \alpha\frac{\partial\theta_w'}{\partial x} = 0, \tag{19}$$

Eq. (16) has additional terms for heat loss and variation of flow rate. Here α_w, α_u, α_c, and α_d represent the speeds of temperature wave fronts in each component. According to Eq. (17) variations of the thermal parameters r_w, r_u, r_e, r_d result in the variation of wave speeds α_w, α_u, α_e, α_d. This important property is used later to explain the results.

3.5 Time Solutions of the Governing Equations. Except the first equation for the collector, the equations in Eq. (16) for other components are solved by the method of Laplace transform. The time solutions for the temperature distributions are

$$\theta_w'(x,\tau) = \exp(-ux/\bar{f}) \left\{ \left[\theta_i' \left(\tau - \frac{x}{\alpha} \right) + \lambda \int_0^{(\tau - x/\alpha)} f'(v)dv \right] \cdot \epsilon(\tau - x/\alpha) - \lambda \int_0^\tau f'(v)dv \right\} \tag{20}$$

where

$$\begin{aligned} &u = u_p, \quad \theta_i' = \theta_2', \quad \lambda = \lambda_u, \quad \alpha = \alpha_u, && \text{riser} \\ &u = u_e, \quad \theta_i' = \theta_3', \quad \lambda = \lambda_e, \quad \alpha = \alpha_e, && \text{exchanger} \\ &u = u_p, \quad \theta_i' = \theta_4', \quad \lambda = \lambda_d, \quad \alpha = \alpha_d, && \text{downcomer} \end{aligned} \tag{21}$$

Here $\epsilon(\tau)$ is the unit step function.

According to the time solution, the temperature at the inlet of each component θ_i' propagates downstream with individual wave speeds. The flow rate $f'(\tau)$ appears in the integration parts. The exponential term in Eq. (20) represents a damping factor. Thus the amplitude of the temperature waves is damped as x proceeds. This damping effect increases with increasing heat loss coefficient u and decreasing flow rate $\bar{f}$. In this case,

the thermosyphon system tends to become more stable. In contrast, if $\bar{f}$ is large or u is small, the damping effect is small and the system tends to become more unstable.

Equation (10) is also solved by Laplace transform to yield the time solution for flow rate:

$$f'(\tau)=\frac{1}{w_{tm}}\exp\left[-\left(\frac{w_{fm}}{w_{tm}}d\bar{f}^{d-1}\right)\tau\right]\cdot\left\{\int_0^\tau\left\{\exp\left[\left(\frac{w_{fm}}{w_{tm}}d\bar{f}^{d-1}\right)v\right]\cdot\left[\oint\theta'(x,v)_w\mathbf{e}_x\cdot\mathbf{e}_z dx\right]\right\}dv\right\}. \quad (22)$$

Here $f'(\tau)$ is determined by integrating the instantaneous thermosyphon head from $\tau=0$ to τ.

An explicit solution of $f'(t)$ is evaluated numerically because of the complexity of the above equations. A finite difference method is used here to solve Eq. (16). According to the von Neumann numerical stability analysis for the hyperbolic-type wave equation, we used the "time-centered implicit" scheme with second-order accuracy, i.e., the *Crank-Nicolson* scheme (Anderson et al., 1984). Several numerical tests using the schemes of unwind, center difference, leap frog, and Crank-Nicolson, etc., were performed. Crank-Nicolson scheme was proved to be the best.

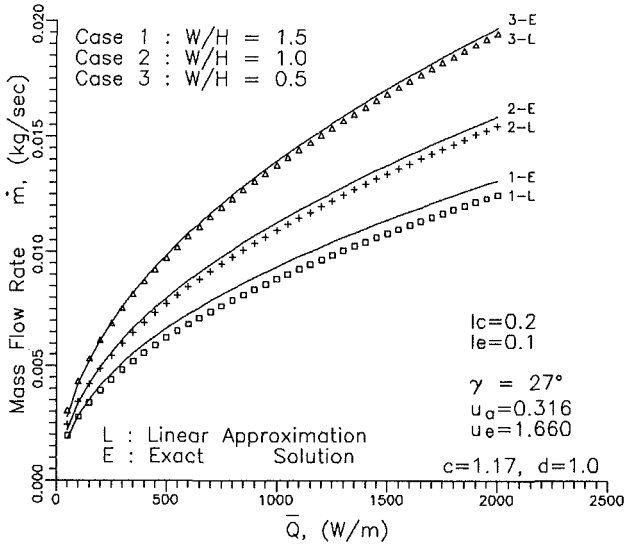

Fig. 2 Solution of the flow rate in the steady-state: comparison between exact solution and linear approximation solution

4 Analytical Results and Discussions

If not stated explicitly, the data presented in Appendix D, which represents a conventional design of solar thermosyphon water heaters commercially available, will be used in the following analysis.

4.1 Steady-State Solution. Equation (11) is an implicit solution for flow rate $\bar{f}$ in the steady state; Eq. (12) is an approximate solution. Both solutions are similar for various $\bar{Q}$ and W/H (aspect ratio of the solar system) (Fig. 2), especially for smaller W/H (i.e., the system is shorter). The approximate solution, Eq. (12), is thus approximately valid. The parameter $\mathcal{A}$ defined in Eq. (12) represents a dimensionless variable to correlate the steady-state flow rate $\bar{f}$ and becomes an important parameter in the following stability analysis.

4.2 Stability Parameters. The system parameters that affect the stability of a solar thermosyphon system are divided into two categories according to the governing Eqs. (5)–(10) and Eq. (22):

(a) the design parameters, including the geometric parameters, l_e, l_c, W/H, and γ; the heat-transfer and friction coefficients u_e, u_a, u_p, and w_{fm}; and the time constants r_p, r_w, r_e, r_u, and r_d. Here, W/H and γ are used for convenience instead of W and H. w_{tm} is included since it is function of the geometric parameters l_e, l_c, W/H, etc.

(b) the operation parameters including the input $\bar{q}$ and the tank temperature $\bar{\theta}_t$ in the steady state.

All the above dimensionless parameters are related to the system stability since they appear in the system dynamics model, Eqs. (13) and (14). However, the three parameters $\bar{q}$, $\bar{\theta}_t$, and w_{fm} can be grouped together to yield a new parameter M which is defined in Eq. (12). To prove this, the neutrally stable value of M are evaluated for three design cases with ($\bar{\theta}_t=0$) or without ($\bar{\theta}_t\neq 0$) heat losses in the tank and varied loop friction. The heat losses from the tank to the surroundings are assumed to be zero ($\bar{\theta}_t=0$) for Cases 1 and 3, the frictional parameters F_{tm} and F_{fm} for Case 3 are twice those in Case 1. The heat loss from the tank is not zero ($\bar{\theta}_t=0.5$) for Case 2, but F_{tm} and F_{fm} for both Cases 1 and 2 are identical.

The neutrally stable curves for three design cases are shown in Fig. 3 to be identical. Other calculations for various designs show the same trend. Hence, M has a similarity property and can be used as a parameter to characterize the stability of a solar thermosyphon system. Therefore, 14 parameters characterize the system stability and the neutrally stable value of M, denoted by M_{cr}, for a given solar system, is written in the form

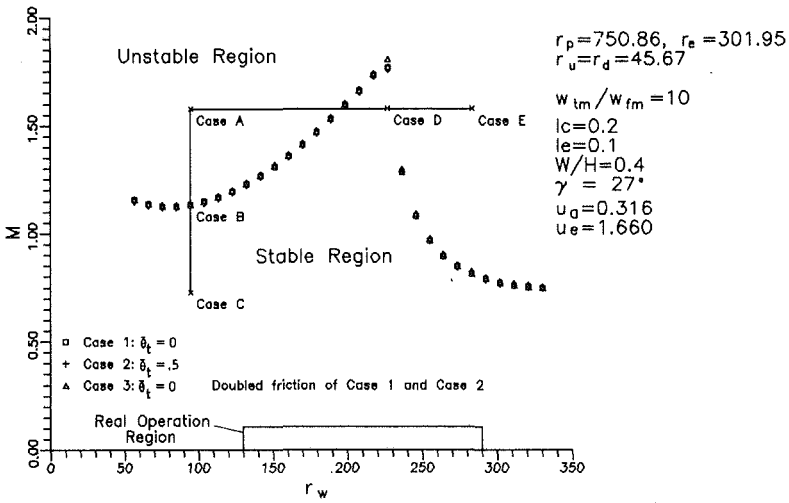

Fig. 3 Effect of r_w

$$M_{cr}\left(l_c, l_e, \frac{W}{H}, \gamma; u_e, u_a, u_p; r_p, r_w, r_e, r_u, r_d, \frac{w_{tm}}{w_{fm}}\right) = 0. \quad (23)$$

A neutrally stable curve is drawn in terms of the function parameters in Eq. (23) that divide the system performance into stable and unstable operation according to the stability map (Fig. 3). M_{cr} represents the maximum permissible flow rate in the steady-state for the solar system to become hydrodynamically stable, since $\bar{f}$ is function of M, Eq. (12). Basically, M represents the operating conditions of the solar system because the functional relation includes terms for solar irradiation and heat loss from the tank. According to Fig. 3, for a system operated at a larger value of M, larger $\bar{f}$ is expected with smaller damping effect (Section 3.5). Hydrodynamic instability occurs when the system parameter M exceeds its critical value M_{cr} ($M \geq M_{cr}$), i.e., when M is located in the unstable region of the stability map. The hydrodynamic stability of a solar thermosyphon water heater is determined by verifying the location of M in a stability map such as Fig. 3.

For fixed M, the heat input $\bar{Q}$ increases with increasing $(\bar{T}_t - T_a)$ and friction factor w_{fm}. Hence, the solar system tends to be unstable for larger solar irradiation ($\bar{q}$ high), smaller tank loss and loop friction (u_a, $\bar{\theta}_t$, w_{fm} small). This result coincides with that of Huang and Zelaya (1987) for a simple rectangular loop.

Regarding the effect of r_w on stability, according to Fig. 3, values of M_{cr} first increase with increasing r_w, then decline after reaching a maximum value. This phenomenon is explained from the numerical solution in the time domain. Flow responses $f'(\tau)$ for five design cases shown in Fig. 3 were carried out to verify the stability for a step input q'. Figure 4 shows that Case C is stable as the oscillation is damped out; Case A is unstable as the amplitude oscillates and increases; Case B is a neutrally stable as oscillation persists. The frequency of the oscillation for unstable cases is about 0.1 rad/s identical with the unstable roots found in the Nyquist analysis.

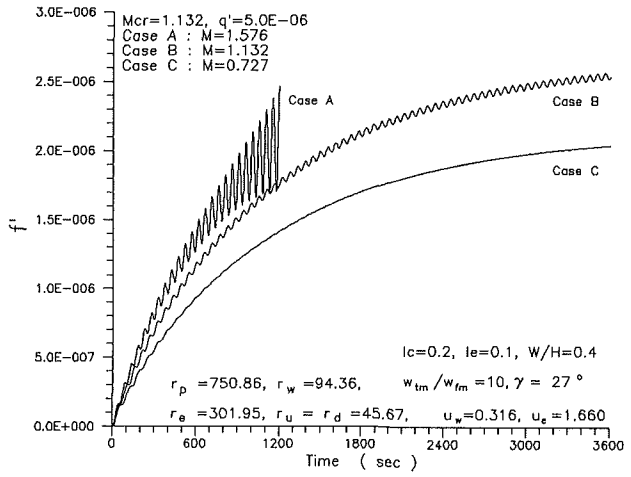

Fig. 4 Numerical solutions in the time domain

The time solutions for Cases A, D, and E are presented in Fig. 5. The solutions for Case A and E reveal unstable oscillations predicted by the stability map in Fig. 3 since the design points are located in the unstable region. The time solution for Case D is stable. The slight oscillation is due to numerical error as the M value for Case D is near M_{cr}. The stability map shown in Fig. 3 is thus verified by the time solutions of Fig. 5.

A maximum value of M_{cr} in the neutrally stable curves of Fig. 3 needs explanation. Welander (1967) found that instability of a thermosyphon loop resulted from the phase difference between the thermosyphon buoyancy and friction forces; both are related to the wave speeds. Variations of r_w alters the wave speed α_w ($=\bar{f}/r_w$). The phase difference between the thermosyphon buoyancy and friction forces is then altered. For given M, continuously increasing r_w results in continuous phase shift from out-of-phase to in-phase, then to out-of-phase mode again ($+2\pi$ from the first out of phase). The operating point thus moves along a line of constant M line from an unstable to stable region, then again to an unstable region (Fig. 3).

From these maps, we can determine the stability of a solar thermosyphon system by comparing the value of M in the operation with M_{cr}. The values of M for most solar water heaters commercially available are calculated here. In practice, the maximum solar irradiation I is about 1200 W/m^2, Q is thus <2400 W/m (for a two-panel collector with standard size 2 m $\times$ 1 m each). For loop friction coefficients chosen from the value determined by Huang et al. (1990) and the design parameters presented in Appendix D, $M \approx 0.073$, which is far below the neutrally stable curve in Fig. 3. The system designed with parameters given in Appendix D is thus in the stable region. Although the operating parameter M may be increased by decreasing the loop friction, the loop friction in practical solar thermosyphon hot water heaters is always finite and cannot be decreased greatly. The practical design of solar ther-

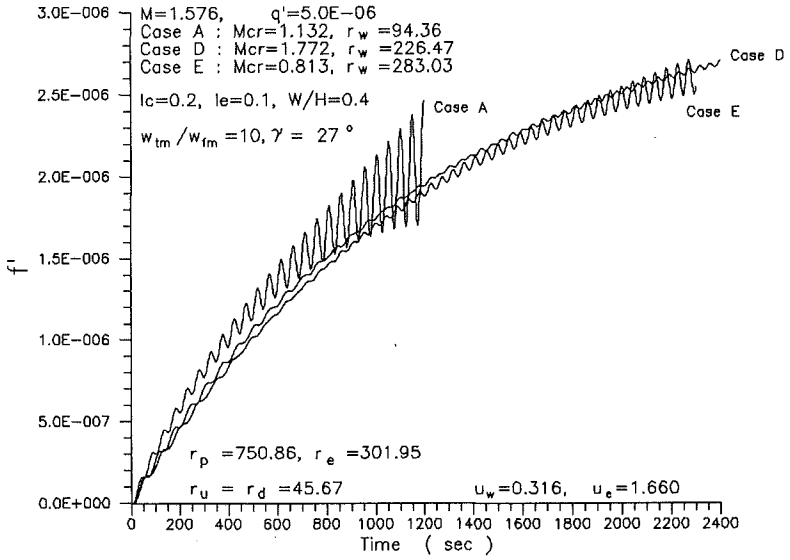

Fig. 5 Numerical solutions in the time domain

mosyphon water heaters cannot diminish more than half the friction presented in Appendix D. This behavior indicates that the values of M of practical solar systems are invariably far below the neutrally stable curve. A hydrodynamic instability is thus unexpected for most solar thermosyphon water heaters.

4.3 Effect of Parameter Variations on Stability. The parametric study of stability for solar thermosyphon systems is complicated according to the characteristic equation, Eq. (23). Here, only two of 14 parameters are varied in a stability map and the others are kept constant. The effects of the latter 12 parameters are discussed separately.

(1) Effect of r_e, r_u, and r_d. The magnitude of parameters, r_e, r_u and r_d affect the wave speeds transferred in the loop. As stated above, the wave speeds vary with the phase differences between the thermosyphon buoyancy and friction forces and also affect the stability. The effect of r_e is shown in Fig. 6. Three design cases were studied. The wavelike stability curve for Case 3 is noted, explained previously, but rapid variation of phase difference results in two maxima for Case 3.

Although r_e in Case 3 is larger than in Cases 1 and 2, the stability curve of Case 3 is not necessarily higher than that of Case 2 because of the variation of wave speeds and phase differences. Although M_{cr} varies rapidly with r_e and r_w, the operating value of M for practical solar water heaters is still far below the neutrally stable curves as shown in Fig. 6. The solar water heaters commercially available are thus invariably hydrodynamically stable.

The effects of r_u and r_d are similar to those of r_w and r_e. As the range of variation are narrow, their stability curves are similar to that in Fig. 3 and are not presented here.

(2) Effect of w_{tm}/w_{fm}. In general, w_{tm} is larger than w_{fm}. Five ratios w_{tm}/w_{fm} were studied. According to Fig. 7, the larger is the ratio w_{tm}/w_{fm}, the lower are the stability curves. Hence, the system tends to become more unstable (the stable region is reduced). This property is indicated by the exponential damping term in Eq. (22). As large ratio w_{tm}/w_{fm} has a small damping effect, the system tends to become more unstable. For Case 5 in Fig. 7, the stability curve is low and the system tends to become more unstable. In practical designs, the ratio w_{tm}/w_{fm} is invariably finite and the values of M for practical operations of thermosyphon water heaters are thus always far below the neutrally stable curves, therefore solar systems are hydrodynamically stable.

(3) Effect of W/H, l_c and l_e. Figure 8 shows the stability curves for four ratios W/H. The larger is the ratio W/H, the higher is the stability curve. Hence, the system tends to be

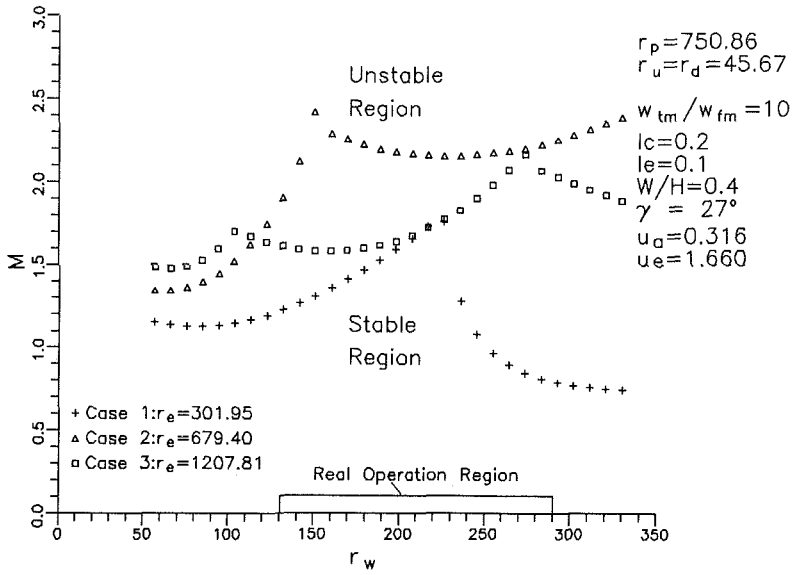

Fig. 6 Effect of r_e

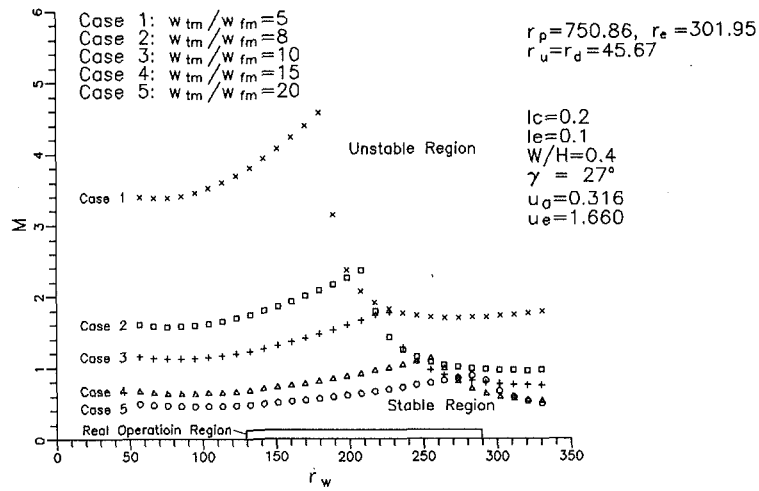

Fig. 7 Effect of w_{tm}/w_{fm}

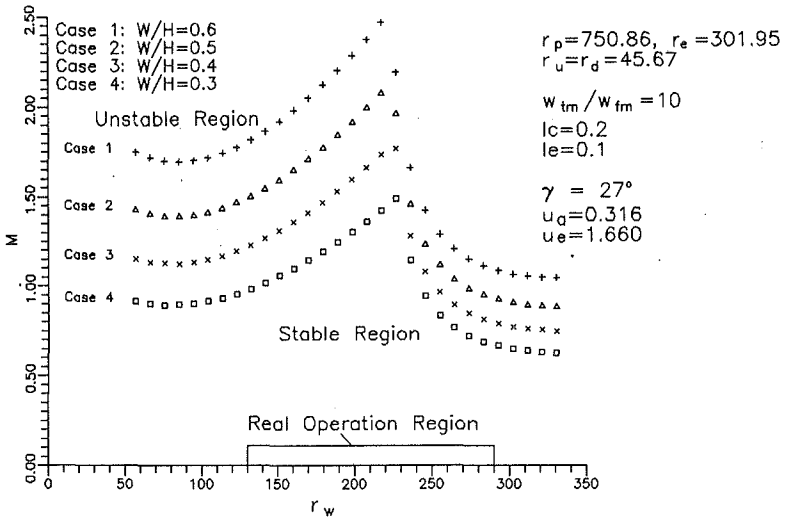

Fig. 8 Effect of *W/H*

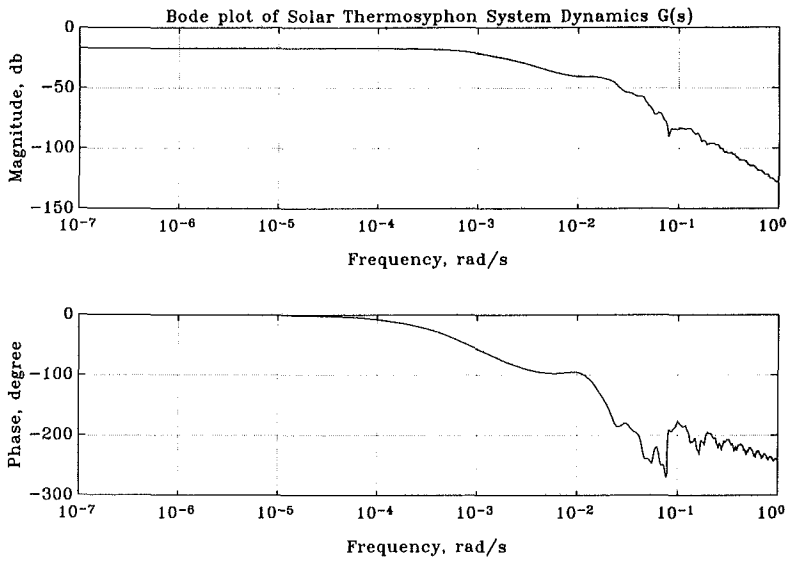

Fig. 9 Bode plot of transfer function *G(s)*

more stable (the stable region is broadened). This behavior coincides with the conclusion of Huang and Zelaya (1987), who found that a larger distance between the heater (collector) and the cooler (exchanger) (larger Δz, smaller W/H) results in a system becoming more unstable. This property is explained by the damping effect in Eq. (20). As a larger Δz results in larger M and larger $\bar{f}$, the damping effect is smaller and the system is more unstable.

The effects of l_c and l_e were examined with a stability map similar to Fig. 6 but not presented here. The solar system is shown to be more stable for larger l_c or l_e because the longer collector or heat exchanger creates a larger damping effect.

The neutrally stable curves (Fig. 8) for various W/H, l_c, and l_e are far above the values of M for practical conditions of most commercial solar water heaters. This property indicates that the solar system is hydrodynamically stable.

(4) Effect of u_e, u_a, r_p and γ. Stability curves for various u_e are similar to Fig. 3 and are not presented here. The system tends to be more stable for larger u_e as the damping effect shown by Eq. (20) is greater for large u_e. Again, most commercial solar water heaters operate at values of M far below the stability curves, hence no flow instability occurs.

The effects of γ, r_p, and u_a on the hydrodynamically stability are minimal since the variation of these parameters is small in practical design. Commercial solar water heaters operate at values of M far below M_{cr}, thus no flow instability occurs.

According to the above discussion, commercial solar water heaters invariably operate at values of M far below the neutrally stable value M_{cr} and are thus invariably hydrodynamically stable. This property is mainly due to larger loop friction and small irradiation in practice.

4.4 System Transfer Model of a Solar System. The dynamic behavior of a solar thermosyphon system is clearly shown by the system dynamics model, Eqs. (13) and (14), using a Bode plot of $G(s)$. The design parameters presented in Appendix D are used in the calculation and the Bode plot presented in Fig. 6 shows that the solar water heater is an overdamped system with low-pass behavior. The gain drops at 20 db/decade approximately for frequencies up to 0.01 rad/s. Furthermore, a more rapidly decreasing rate is seen at frequencies greater than 0.01 rad/s. The phase lag approaches -100 deg at $\omega = 0.01$ rad/s, and -270 deg at $\omega > 0.1$ rad/s. Hence, the dynamic behavior of the solar system is approximately second order with a delay at frequency $\omega \leq 0.01$ rad/s, but alters to a system of higher order at frequency $\omega > 0.1$ rad/s. Nevertheless, the dynamic system is stable.

According to this typical Bode plot, the upper limit frequency (< 0.5 rad/s) used in Section 3.3 to map s contour to

$G_d(s)$ plane is adequate. Although unstable roots may exist in a region of higher frequency, this possibility can be ignored since the system possesses low-pass properties and the gain drops to a value much smaller than -40 db. Morrison et al. (1980) showed that a step variation of solar radiation to a thermosyphon hot water system resulted in a low-frequency oscillation of flow that was rapidly damped. The system was shown to be stable similar to the present case shown in Fig. 9.

5 Conclusion

Reverse flow commonly observed in solar thermosyphon water heaters was suspected to be due to hydrodynamic instability. A theoretical analysis was carried out with a one-dimensional approach and a linear perturbation method to derive a system dynamics model. A transfer function that treats solar irradiation as the system input and flow rate as the system output was derived to describe the dynamic behavior of solar thermosyphon water heaters. The characteristic equation was then obtained and the Nyquist criterion was used to examine the flow instability. According to the governing equations and the steady-state solutions, the parameter M can be a dimensionless parameter for system stability. The stability maps are then plotted in terms of 14 parameters. The occurrence of hydrodynamic stability is determined by comparing the stability curves with the designed values of M. Flow instability cannot occur in most solar water heaters commercially available, because the loop friction is high in the design and solar irradiation in field operation is still not great enough to cause flow instability. The reverse flow observed in some solar thermosyphon water heaters is shown not to be due to hydrodynamic instability, it may be caused by thermosyphon saturation.

Acknowledgment

The present study was supported by Energy Commission, Ministry of Economic Affairs, Taiwan, R.O.C. through Grant No. 782J1 and by National Science Council of the Republic of China, through Grant No. NSC78-0401-E002-18.

References

Anderson, D. A., Tannehill, J. C., and Pletcher, R. H., 1984, *Computational Fluid Mechanics and Heat Transfer*, McGraw-Hill, New York.

Bau, H. H., and Torrance, K. E., 1981, "On the Stability and Flow Reversal of an Asymmetrically-Heated Open Convection Loop," *J. Fluid Mech.*, Vol. 106, pp. 417-433.

Creveling, H. F., De Paz, J. F., Baladi, J. Y., and Schoenhals, R. J., 1975, "Stability Characteristics of a Single-Phase Free Convection Loop," *J. Fluid Mech.*, Vol. 67, Part 1, pp. 65-84.

Greif, R., 1988, "Natural Circulation Loops," ASME *Journal of Heat Transfer*, Vol. 110, pp. 1243-1258.

Huang, B. J., and Hsieh, C. T., 1985, "A Simulation Method for Solar Thermosyphon Collector," *Solar Energy*, Vol. 35, pp. 31-43.

Huang, B. J., and Zelaya, R., 1987, "Stability Analysis of a Thermosyphon Loop," *ISES Solar World Congress*, Hamburg.

Keller, J. B., 1966, "Periodic Oscillations in a Model of Thermal Convection," *J. Fluid Mech.*, Vol. 26, Part 3, pp. 599-606.

Mertol, A., Place, W., and Webster, T., 1981, "Detailed Loop Model (DLM) Analysis of Liquid Solar Thermosyphons with Heat Exchangers," *Solar Energy*, Vol. 27, No. 5, pp. 367-386.

Morrison, G. L., and Ranatunga, D. B. J., 1980, "Transient Response of Thermosyphon Solar Collectors," *Solar Energy*, Vol. 24, pp. 55-61.

Morrison, G. L., 1986, 'Reverse Circulation in Thermosyphon Solar Water Heaters," *Solar Energy*, Vol. 36, No. 4, pp. 373-379.

Ong, K. S., 1974, "A Finite-Difference Method to Evaluate the Thermal Performance of Solar Water Heater," *Solar Energy*, Vol. 16, pp. 137-147.

Vaxman, M., and Sokolov, M., 1986, "Effects of Connecting Pipes in Thermosyphonic Solar Systems," *Solar Energy*, Vol. 37, No. 5, pp. 323-330.

Welander, Pierre, 1967, "On the Oscillatory Instability of a Differentially Heated Loop," *J. Fluid Mech.*, Vol. 29, pp. 17-30.

Zvirin, Y., Shitzer, A., and Grossman, G., 1977, "The Natural Circulation Solar Heaters—Models with Linear and Nonlinear Temperature Distributions," *Int. J. Heat Mass Transfer*, Vol. 20, pp. 997-999.

Zvirin, Y., Shitzer, A., and Bartal-Bornstein, A., 1978, "On the Stability of the Natural Circulation Solar Heater," *Proc. 6th Int. Heat Transfer Conference*, Toronto, Canada.

Zvirin, Y., and Greif, R., 1979, "Transient Behavior of Natural Circulation Loops: Two Vertical Branches with Point Heat Source and Sink," *Int. J. Heat Mass Transfer*, Vol. 22, pp. 499-504.

APPENDIX A

Definitions of Parameters and Dimensionless Variables

$$\psi_p=\frac{\rho_p A_p C_{pp}}{U_w};\quad \psi_w=\frac{\rho_w A_w C_{pw}}{U_w};\quad \psi_e=\frac{\rho_w A_e C_{pw}}{U_w};$$

$$\psi_u=\frac{\rho_w A_u C_{pw}}{U_w};\quad \psi_d=\frac{\rho_w A_d C_{pw}}{U_w} \tag{A1}$$

$$T_{\text{ref}}=\frac{\overline{Q}}{U_w};\quad q=\frac{Q}{T_{\text{ref}}U_w};\quad \theta=\frac{T-T_a}{T_{\text{ref}}};\quad x=\frac{y}{L_s};\quad l=\frac{L}{L_s};$$

$$u_a=\frac{U_a}{U_w};\quad u_e=\frac{U_e}{U_w};\quad u_p=\frac{U_p}{U_w} \tag{A2}$$

$$\tau=\frac{t}{t_{\text{ref}}};\quad r_p=\frac{\psi_p}{t_{\text{ref}}};\quad r_w=\frac{\psi_w}{t_{\text{ref}}};\quad r_e=\frac{\psi_e}{t_{\text{ref}}};\quad r_u=\frac{\psi_u}{t_{\text{ref}}};\quad r_d=\frac{\psi_d}{t_{\text{ref}}} \tag{A3}$$

$$f=\frac{\dot{m}C_{pw}}{U_w L_s},\quad w_{tm}=\frac{F_{tm}U_w}{C_{pw}\cdot t_{\text{ref}}\cdot T_{\text{ref}}},\quad w_{fm}=\frac{F_{fm}\left(\frac{U_w L_s}{C_{pw}}\right)^d}{T_{\text{ref}}\cdot L_s}. \tag{A4}$$

APPENDIX B

Relations of Parameters and Coefficients in the Steady-State Solution (11)

$$\overline{h}_c(\bar{f})=\left\{\frac{\bar{f}(1+u_a)}{u_a}(1-b_1)\left[\bar{\theta}_1-\frac{\bar{q}}{u_a}\right]+\frac{l_c\cdot\bar{q}}{u_a}\right\}(\sin\gamma);$$

$$\overline{h}_u(\bar{f})=\bar{\theta}_2\frac{\bar{f}}{u_p}(1-b_5) \tag{B1}$$

$$\overline{h}_e(\bar{f})=\frac{\bar{f}}{u_e}(1-b_3)(\bar{\theta}_3-\bar{\theta}_t)+\bar{\theta}_t l_e;\quad \overline{h}_d(\bar{f})=\bar{\theta}_4\frac{\bar{f}}{u_p}(1-b_6) \tag{B2}$$

$$\bar{\theta}_1=\{\bar{q}/u_a(1-b_1)\cdot b_2\cdot b_3\cdot b_4+\bar{\theta}_t(1-b_3)\cdot b_4\}/(1-b_1\cdot b_2\cdot b_3\cdot b_4) \tag{B3}$$

$$\bar{\theta}_2=\{\bar{q}/u_a(1-b_1)+\bar{\theta}_t\cdot b_1\cdot(1-b_3)\cdot b_4\}/(1-b_1\cdot b_2\cdot b_3\cdot b_4) \tag{B4}$$

$$\bar{\theta}_3=\{\bar{q}/u_a(1-b_1)\cdot b_2+\bar{\theta}_t\cdot b_1\cdot b_2\cdot(1-b_3)\cdot b_4\}/(1-b_1\cdot b_2\cdot b_3\cdot b_4) \tag{B5}$$

$$\bar{\theta}_4=\{\bar{q}/u_a(1-b_1)\cdot b_2\cdot b_3+\bar{\theta}_t(1-b_3)\}/(1-b_1\cdot b_2\cdot b_3\cdot b_4) \tag{B6}$$

$$b_1=\exp\{-u_a l_c/[\bar{f}(1+u_a)]\};\quad b_2=\exp(-u_p l_u/\bar{f});$$

$$b_3=\exp(-u_e l_e/\bar{f}). \tag{B7}$$

$$b_4=\exp(-u_p l_d/\bar{f});\quad b_5=\exp(-u_p l_{uv}/\bar{f});\quad b_6=\exp(-u_p l_{dv}/\bar{f}) \tag{B8}$$

APPENDIX C

Definitions of Parameters in Eqs. (13) and (14)

$$k_1=\frac{u_a}{\bar{f}(1+u_a)}[\bar{\theta}_1-\bar{q}/u_a];\quad k_2=\bar{\theta}_2 u_p/\bar{f};$$

$$k_3=u_e(\bar{\theta}_3-\bar{\theta}_t)/\bar{f};\quad k_4=\bar{\theta}_4 u_p/\bar{f} \tag{C1}$$

$$c_1 = r_w r_p s^2 + [r_w(u_a+1) + r_p]s + u_a;$$

$$c_2 = r_p s + (u_a+1); \quad c_3 = c_4 \cdot s \tag{C2}$$

$$c_4 = r_w r_p (1+u_a)s + [r_w(1+u_a)^2 + r_p]; \quad c_5 = r_u s + u_p;$$

$$c_6 = r_e s + u_e; \quad c_7 = r_d s + u_p \tag{C3}$$

$$\theta_1'(s) = [(c_1 z_3)\cdot f' + (c_3 v_3)\cdot q']/z_1;$$

$$\theta_2'(s) = [(c_1 z_4)\cdot f' + (c_3 v_4)\cdot q']/z_1 \tag{C4}$$

$$\theta_3'(s) = [(c_1 z_5)\cdot f' + (c_3 v_5)\cdot q']/z_1;$$

$$\theta_4'(s) = [(c_1 z_6)\cdot f' + (c_3 v_6)\cdot q']/z_1 \tag{C5}$$

$$v_3 = (1-p_1)p_2 p_3 p_4; \quad v_4 = (1-p_1);$$

$$v_5 = (1-p_1)p_2; \quad v_6 = (1-p_1)p_2 p_3 \tag{C6}$$

$$p_1 = \exp[-(c_1 l_c)/(\bar{f} c_2)]; \quad p_2 = \exp(-c_5 l_u/\bar{f});$$

$$p_3 = \exp(-c_6 l_e/\bar{f}); \tag{C7}$$

$$p_4 = \exp(-c_7 l_d/\bar{f}); \quad p_5 = \exp(-c_5 l_{uv}/\bar{f}); \quad p_6 = \exp(-c_7 l_{dv}/\bar{f}) \tag{C8}$$

$$z_1 = (1 - p_1 p_2 p_3 p_4) c_1 c_3 \tag{C9}$$

$$z_3 = k_1 c_2 (1+u_a)(b_1 - p_1) p_2 p_3 p_4 + \left[\frac{k_2}{r_u}(b_2 - p_2) p_3 p_4 + \frac{k_3}{r_e}(b_3 - p_3) p_4 + \frac{k_4}{r_d}(b_4 - p_4)\right] c_4 \tag{C10}$$

$$z_4 = k_1 c_2 (1+u_a)(b_1 - p_1) + p_1 \left[\frac{k_2}{r_u}(b_2 - p_2) p_3 p_4 + \frac{k_3}{r_e}(b_3 - p_3) p_4 + \frac{k_4}{r_d}(b_4 - p_4)\right] c_4 \tag{C11}$$

$$z_5 = p_1 p_2 \left\{\frac{k_3}{r_e}(b_3 - p_3) p_4 + \frac{k_4}{r_d}(b_4 - p_4)\right\} c_4 + k_1 c_2 (1+u_a)(b_1 - p_1) p_2 + \frac{k_2}{r_u}(b_2 - p_2) c_4 \tag{C12}$$

$$z_6 = p_1 p_2 p_3 \frac{k_4}{r_d}(b_4 - p_4) c_4 + k_1 c_2 (1+u_a)(b_1 - p_1) p_2 p_3 + \frac{k_2}{r_u}(b_2 - p_2) p_3 c_4 + \frac{k_3}{r_e}(b_3 - p_3) c_4 \tag{C13}$$

$$h_c' = \left\{z_3 \bar{f} c_2 (1-p_1) + k_1 c_2 (1+u_a)\left[\frac{\bar{f}(1+u_a)}{u_a}(1-b_1) c_1 - \bar{f} c_2 (1-p_1)\right](1 - p_1 p_2 p_3 p_4)\right\} \cdot c_5 c_6 c_7 \sin\gamma \tag{C14}$$

$$h_u' = \left\{z_4 \bar{f}(1-p_5) + \frac{k_2}{r_u}\left[\frac{\bar{f}}{u_p}(1-b_5) c_5 - \bar{f}(1-p_5)\right] c_4 (1 - p_1 p_2 p_3 p_4)\right\} c_1 c_6 c_7 \tag{C15}$$

$$h_e' = \left\{z_5 \bar{f}(1-p_3) + \frac{k_3}{r_e}\left[\frac{\bar{f}(1-b_3)}{u_e} c_6 - \bar{f}(1-p_3)\right] c_4 (1 - p_1 p_2 p_3 p_4)\right\} c_1 c_5 c_7 \tag{C16}$$

$$h_d' = \left\{z_6 \bar{f}(1-p_6) + \frac{k_4}{r_d}\left[\frac{\bar{f}(1-b_6)}{u_p} c_7 - \bar{f}(1-p_6)\right] c_4 (1 - p_1 p_2 p_3 p_4)\right\} c_1 c_5 c_6 \tag{C17}$$

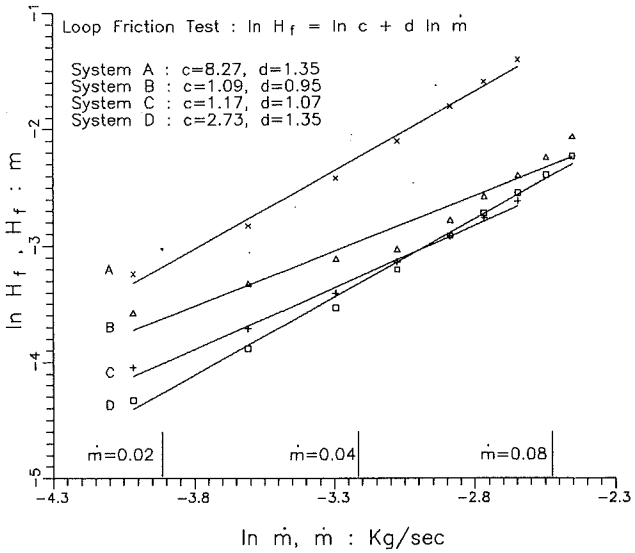

Fig. 1A Friction loss head

$$h_{qc}' = \sin\gamma \left\{(1-p_1)^2 p_2 p_3 p_4 \bar{f} c_2 + \left[l_c c_1 - \bar{f} c_2 (1-p_1)\right](1 - p_1 p_2 p_3 p_4)\right\} c_5 c_6 c_7 \tag{C18}$$

$$h_{qu}' = (1-p_1)(1-p_5)\bar{f} c_1 c_6 c_7 \tag{C19}$$

$$h_{qe}' = (1-p_1)(1-p_3) p_2 \bar{f} c_1 c_5 c_7 \tag{C20}$$

$$h_{qd}' = (1-p_1)(1-p_6) p_2 p_3 \bar{f} c_1 c_5 c_6 \tag{C21}$$

APPENDIX D

System Design Data

The working fluid in the loop is water. The basic data for the design parameters are given here.

(1) U_a and U_w.

The heat-transfer coefficients, U_a and U_w, are evaluated from the collector test results according to ANSI/ASHRAE 93-1986 Standard. As quasi-steady U_a and U_w is assumed, by comparing the steady-state terms of the energy equation with the Hottel-Whillier-Bliss equation, we obtain

$$U_a = \frac{A_c U_L}{L_c}; \quad U_w = \frac{F'}{1-F'}\left(\frac{A_c U_L}{L_c}\right) \tag{D1}$$

where F' and U_L are related to the parameter, $F_R(\tau\alpha)_n$ and $F_R U_L$, defined in the Hottel-Whillier-Bliss equation through the following relation:

$$F' U_L = -G_o C_{pw} \ln\left\{1 - \frac{F_R U_L}{G_o C_{pw}}\right\};$$

$$F'(\tau\alpha)_n = \frac{F_R(\tau\alpha)_n}{F_R U_L} F' U_L \tag{D2}$$

where G_o is the mass flow rate per unit area of collector. $(\tau\alpha)_n$ is the transmittance-absorptance product of the collector at solar noon. For the solar collector commercially available that we used, $F_R(\tau\alpha)_n = 0.642$, $F_R U_L = 4.22$ W/m^2 °C, $A_c = 3.785$ m^2, $L_c = 1.96$ m, and $(\tau\alpha)_n = 0.85$. Hence, $U_a = 11.0$ W/m °C and $U_w = 34.8$ W/m °C.

(2) U_p.

For simplification, we neglect the heat loss from riser and downcomer, i.e., $U_p = 0$.

(3) U_e.

Assume that there are n_e tubes in the exchanger, that the flow is a fully developed laminar in the tubes, and that the tank temperature is constant. We have Nusselt number $N_u = 3.66$ from convection theory; hence $U_e = 7.2 \cdot n_e$ W/m °C. Here the thermal conductivity of water is taken as 0.628 W/m °C (at 40°C). With $n_e = 8$, $U_e = 57.6$ W/m °C.

(4) c and d in frictional loss head H_f.

The frictional loss tests for four typical solar thermosyphon water heaters were measured (Fig. A1). For System C, $c = 1.17$, $d = 1.07$. For simplicity, let $d = 1$.

(5) Other design parameters.

$$L_s = 10 \text{ m}, \quad L_c/L_s = 0.2, \quad L_e/L_s = 0.1, \quad W/H = 0.4,$$
$$\gamma = 27 \text{ deg}, \quad T_a = 20°\text{C}, \quad T_t = 20°\text{C}, \quad \rho_p A_p = 30 \text{ kg/m},$$
$$C_{pp} = 870 \text{ J/kg °C}. \quad A_w = 0.00157 \text{ m}^2,$$
$$A_u = A_d = 0.00038 \text{ m}^2, \quad A_e = 0.00251 \text{ m}^2.$$